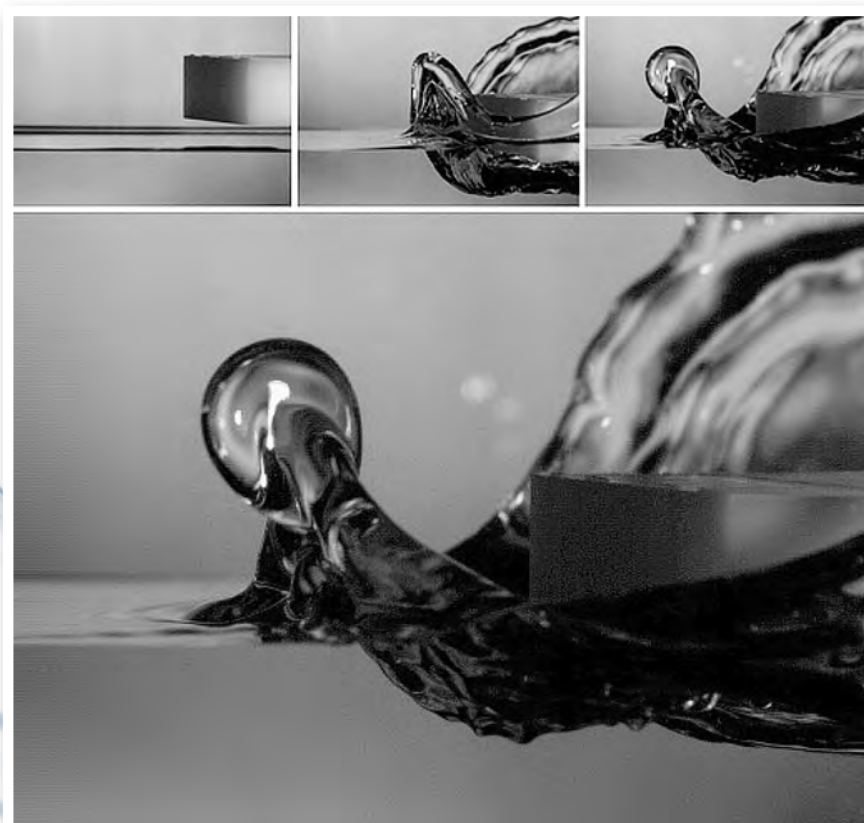


March 2014

Volume 26 Number 3

# AIP | Physics of Fluids



[pof.aip.org](http://pof.aip.org)

## Singular structures on liquid rims

Hans C. Mayer and Rouslan Krechetnikov

*Department of Mechanical Engineering, University of California, Santa Barbara, California 93106, USA*

(Received 5 November 2013; accepted 27 February 2014; published online 28 March 2014)

This experimental note is concerned with a new effect we discovered in the course of studying water hammering phenomena. Namely, the ejecta originating from the solid plate impact on a water surface brings about a liquid rim at its edge with the fluid flowing towards the rim center and forming a singular structure resembling a “pancake.” Here, we present the experimental observations and a qualitative physical explanation for the effect, which proves to be fundamental to the situation when the size and speed of the impacting body are such that the capillary effects become important. © 2014 AIP Publishing LLC. [<http://dx.doi.org/10.1063/1.4868730>]

The interplay of the continuous and the discrete is intrinsic in the description of the world – the emergence of discrete structures from continuous data has always been fascinating to scientists not only for its visual appeal but also for its fundamental importance.<sup>1</sup> In the present work, we will discuss a particular exhibition of such phenomena due to the competition between inertia and surface tension effects. Namely, in the course of water hammering experiments, cf. Figure 1, we observed a phenomenon which resembles a “pancake” formed on liquid rims, a well-developed case of which is illustrated in Figure 2. Its formation in time is shown in Figure 3, where one can observe how the ejecta grows, a liquid rim forms at its end due to retraction, and finally a pancake appears.

There are a few *key questions* originating from these observations. First, (I) what makes the fluid flow towards the center of the rim thus leading to the formation of the pancake structure? Second, we observed that the pancake preferably forms along the shorter side of the impacting plate, which brings the related questions as to (II) why does ejecta develop higher along the long side of the impactor compared to that along the shorter side of the impactor as one can infer from Figure 3(a)? Also, (III) why does the ejecta develop higher along the sides of the impactor compared to the ejecta originating from under the corner as can be seen from both Figures 2 and 3? All these questions stimulated a more systematic study of this interesting phenomenon to be discussed below.

For the measurements, we used rectangular impactor plates with the same long side of  $2l = 63.5$  mm, but the short side was varied in the range  $w = 15.9 - 28.6$  mm; the impact depths explored were in the range  $h = 0.5 - 2$  mm and the impact velocities  $V_0 = 380 - 700$  mm/s. In order to find the transitions between the “no pancake” and “pancake” regimes, we fixed the impactor width and impact depth and then spun the impact velocity. While visually it is obvious what one may call a “pancake,” cf. Figure 2, for a systematic analysis of the data we called the structure in the middle of the rim a “pancake” if its diameter is at least 1.5 that of the rim and if by the time of its formation at least half of it is above the undisturbed water level.

The results of our findings are summarized in Figure 4, which shows the transition measurements in the space defined by the impact velocity  $V_0$  and impactor width  $w$ . Two types of transitions – “no pancake to pancake” (np-p) and “pancake to corrugations” (p-c) – were identified as illustrated in Figure 4(a) for impact depth 1 mm. Figure 4(b) reflects the effect of the impact depth on the transition from “no pancake to pancake.” There are a few key trends to point out. Generally, in the order of increasing impact speed  $V_0$ , one goes through the regimes of “no pancake,” “pancake,” and “corrugations,” cf. Figure 4(a); the increase in the depth of impact  $h$  shifts the transition from “no pancake to pancake” to lower values of  $V_0$ , cf. Figure 4(b). As one can see in Figure 4(a), the

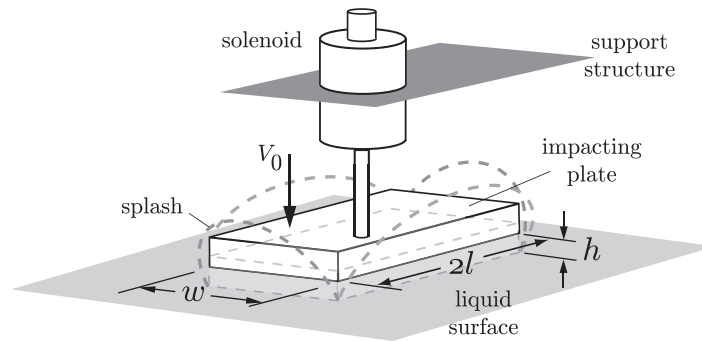


FIG. 1. Experimental apparatus used to produce “pancake” structures on liquid rims. The impacting plate of width  $w$  and length  $2l > w$  is connected to the plunger of a solenoid. When the solenoid is actuated by a laboratory power supply, the plate is set into motion and impacts the liquid surface with a speed  $V_0$  (adjusted through the power supply voltage) creating the splash (shown as dashed lines). The depth of impact  $h$  can be varied via the support structure. Impact events are filmed with a high-speed digital camera (Phantom v5.2) and side lighting from a LED source (IDT).

pancake formation takes place over a narrow range of velocities, in between the transition from “no pancake to pancake” and “pancake to corrugations,” which explains the rarity of the phenomenon.

Next, the difference between the liquid rim radius at the apex of the ejecta evolution versus the maximum pancake diameter over the entire course of the ejecta evolution as functions of the impact velocity  $V_0$  is shown in Figure 5. Figure 5(a) suggests that the rim diameter at the apex of ejecta elevation increases with the impact depth, and Figure 5(b) indicates that for a fixed depth  $h$  the rim diameter is not a strong function of the impact speed  $V_0$  and plate width  $w$ , but for deeper impacts, e.g., depth of 2 mm, the wider plates lead to larger pancakes, cf. Figure 5(a).

With all these data reported, the idea now is to develop basic physical intuition about the observed trends summarized above as well as to answer the key questions (I)–(III). First, note that based on the incompressible pressure-impulse theory,<sup>2</sup> the gauge pressure-impulse distribution across the plate is given by  $\int_{-0}^{+0} p dt = \rho V_0 \sqrt{l^2 - x^2}$ , where  $x = 0$  corresponds to the plate center  $O$  and  $x = l$  to the plate edge  $S$ , cf. Figure 6. Thus, the pressure gradient driving fluid from under

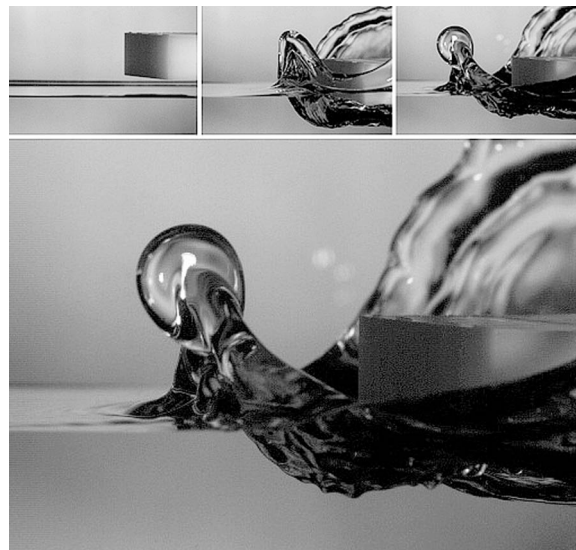


FIG. 2. Sequence of events leading to the pancake (46.7 ms after the impact) formed along the shorter side of the impactor of size  $25.4 \times 63.5$  mm (impact depth 2 mm and velocity  $V_0 = 528$  mm/s).

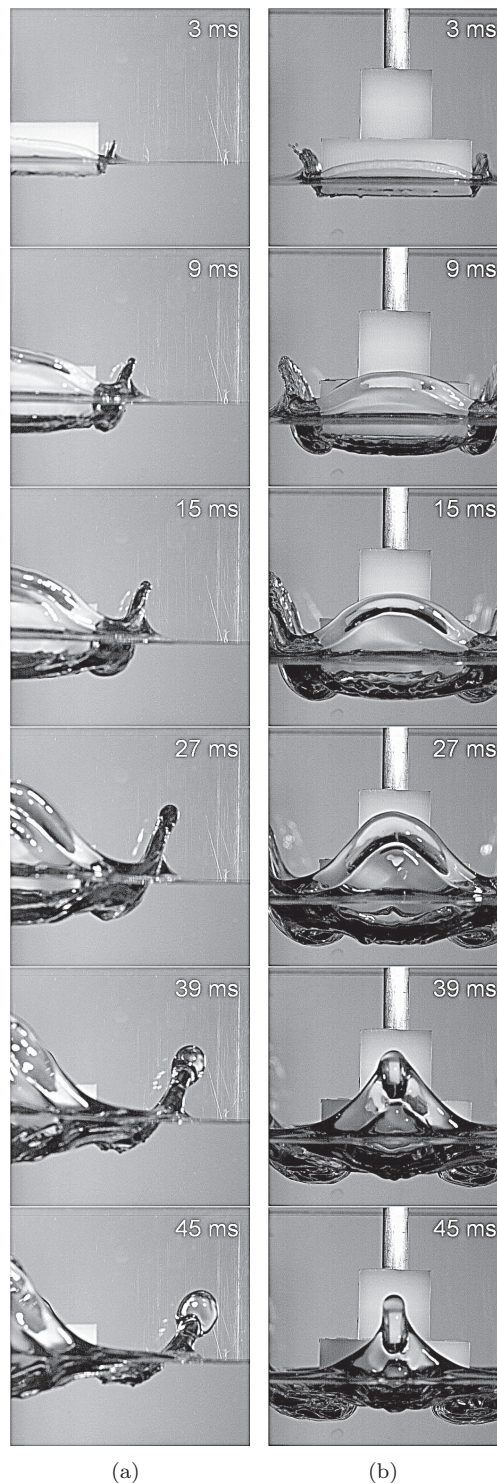


FIG. 3. Time sequence of side (a) and front (b) views of the “pancake” structure evolution (the impact conditions are given in the caption of Figure 2).

the center  $O$  of the impactor to the edge is higher for the fluid flowing towards the long side of the impactor  $L$  compared to the shorter side  $S$ , which entails differences in the ejecta velocity and thus answers question (II). Similarly (question (III)), in part the ejecta raises more along the impactor sides because the pressure gradient driving fluid (wall jet) from under the center of the impactor is

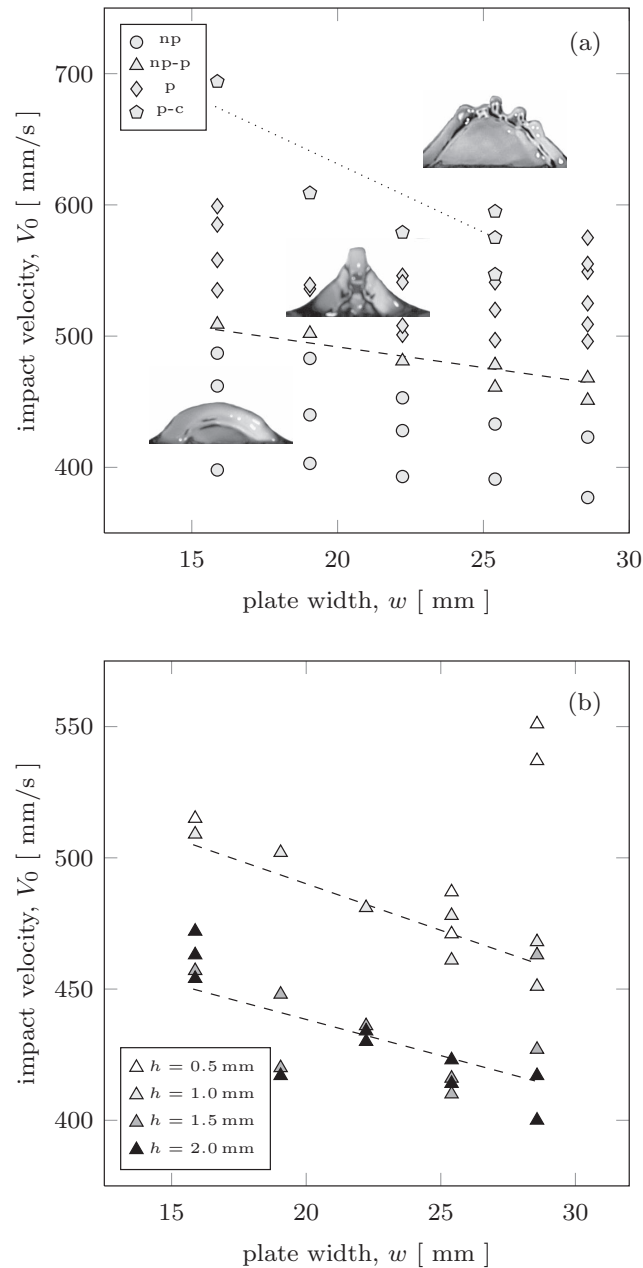


FIG. 4. Measurements of the transition (np-p) from “no pancake to pancake” in the space defined by the impact velocity  $V_0$  versus impactor width  $w$ : (a) two types of transitions – “no pancake to pancake” (np-p) and “pancake to corrugations” (p-c) for impact depth  $h = 1.0$  mm; (b) effect of the impact depth  $h$  on the transition from “no pancake to pancake” (np-p) – deeper impacts shift the transition to lower velocities  $V_0$ . The dashed and dotted lines are provided only to guide the eye.

higher for the fluid flowing towards the edges  $S$ ,  $L$  of the impactor compared to that towards the corner  $C$ . Also, one may think in terms of the high curvature  $\kappa$  of the corner and its analogy to the impact of a small radius  $\kappa^{-1}$  disk, which would not produce as much ejecta due to surface tension  $\sigma$  domination over inertia,  $\rho V_0^2 / (\kappa \sigma) \ll 1$ . Finally, concerning question (I), since the velocity at the corner  $V_c$  is lower compared to that at the center  $V_s$ , the pressure at the corner is higher,  $p_c > p_s$ , and thus there must be fluid flow towards the center of the edge  $S$  and hence up along the rim, cf. Figure 6 – this is supported by the Particle Image Velocimetry (PIV) fields in Figure 7. Next, during its formation, the ejecta continuously retracts due to surface tension and forms a rim at its edge. In

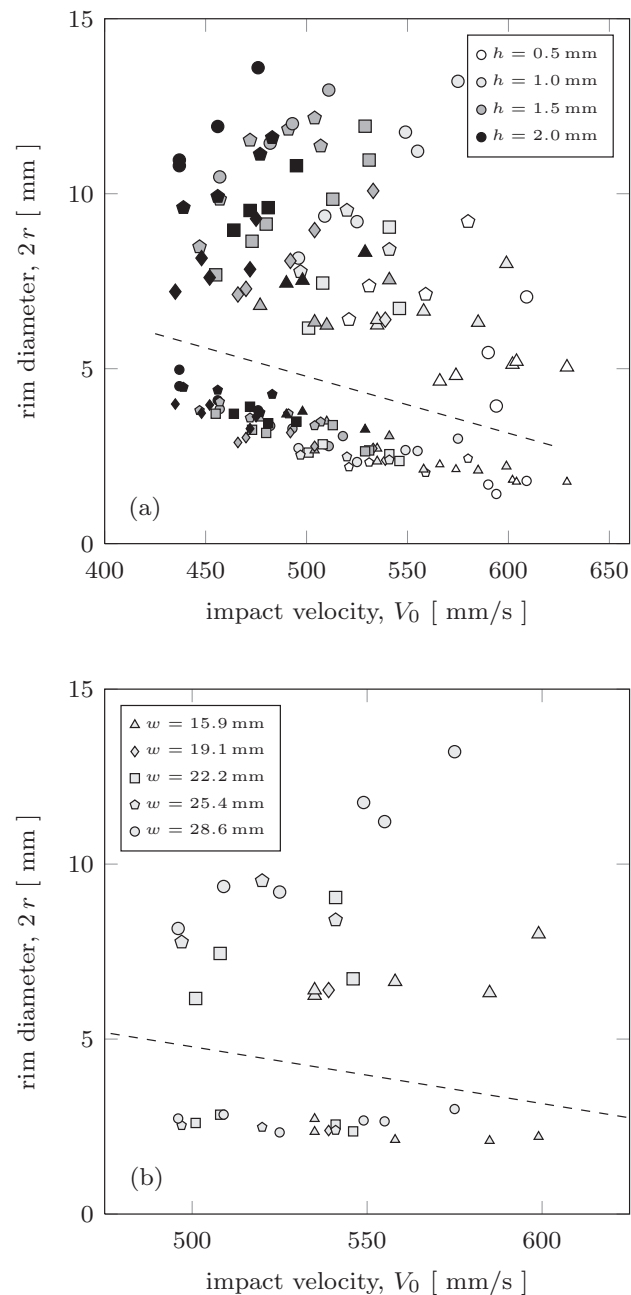


FIG. 5. Liquid rim diameter (smaller symbols) at the apex of the ejecta evolution versus maximum pancake diameter (larger symbols) over the course of the ejecta evolution as functions of the impact velocity  $V_0$  (marker symbols differentiate plate width  $w$  as given in the legend to part (b)): (a) effect of the impact depth  $h$ ; (b) effect of the impactor width  $w$  for the depth fixed at  $h = 1.0$  mm.

this context, a pancake forms if the fluid flux ( $\sim V_r$ ) from under the plate along the rim towards its center overcomes the mass flux to the rim due to the ejecta retraction.

While the above explains the mechanism behind the pancake origin, let us determine the conditions for the transitions “np-p” and “p-c” in Figure 4 with the help of a qualitative model formulated based on first principles. Because of the intrinsic difficulty<sup>3</sup> of the problem, from the point of view of analytical treatment, no attempt will be made to develop a scaling capable of collapsing the data; instead, we will focus on developing a simple model only as a means to provide

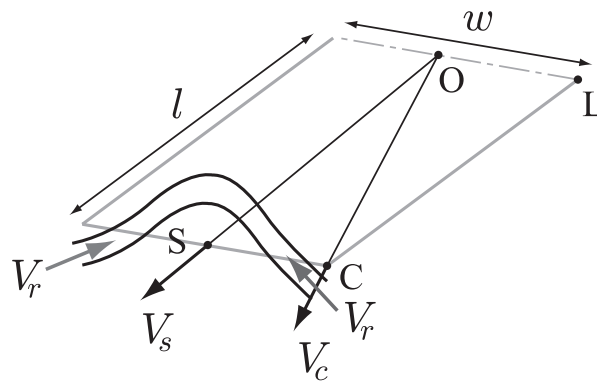


FIG. 6. On the origin of the pancake (plate is of  $w \times 2l$  size; half of the plate is shown).

a minimal physical explanation of the phenomena, in particular the “np-p” and “p-c” transitions. In view of that, we will consider the ejecta formed along the short side of the impactor of width  $w < 2l$  as two-dimensional (2D), i.e., we will calculate all quantities per unit length. Denoting the depth of impact by  $h$ , ejecta thickness  $\delta$ , its height  $H$  (unaffected by retraction due to surface tension) and initial velocity  $V_e$  of the mass (wall jet) contributing to the ejecta, we can write down mass,

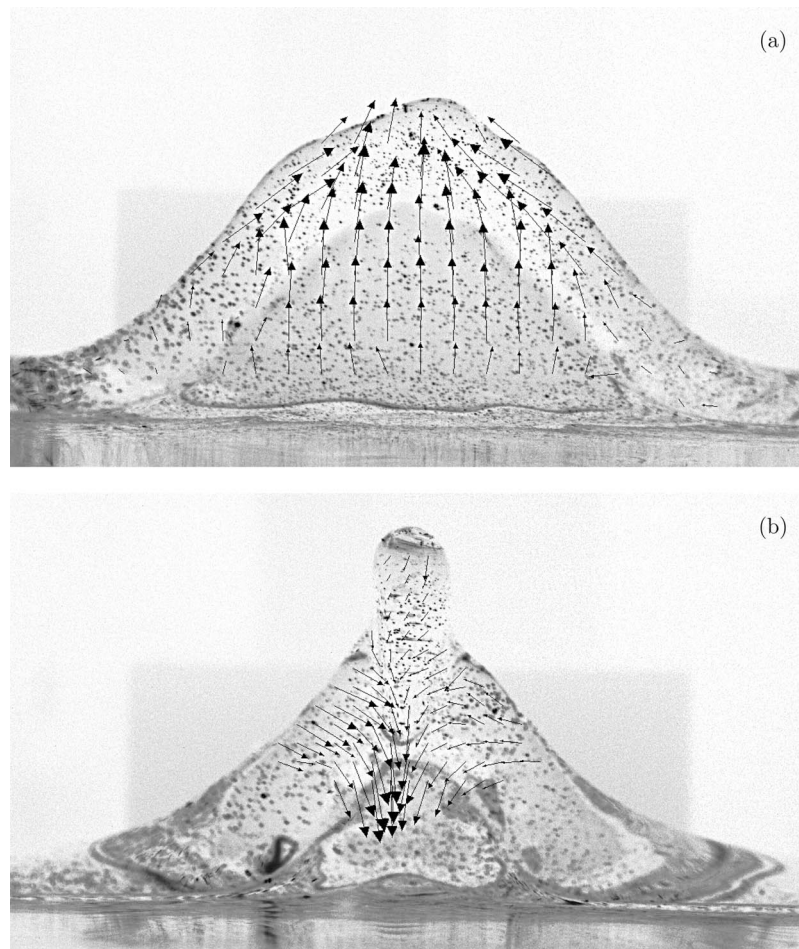


FIG. 7. PIV fields of the front view: (a) rim stage; (b) pancake stage. Only qualitative information on the velocity field is provided due to the curved interface.

linear momentum, and energy conservation. The mass balance hinges on the assumption that all the displaced fluid goes into the ejecta

$$2lh = 2\delta H. \quad (1)$$

In the linear momentum balance, the momentum of the added mass per unit length, which equals to a half-cylinder<sup>4</sup> of diameter  $l$ , i.e.,  $\rho \pi l^2/2$ , and that of due to penetration of the plate at depth  $h$  goes into the momentum of the ejecta

$$\rho \left( \frac{\pi}{2} l^2 + 2lh \right) V_0 = \rho \delta H V_e. \quad (2)$$

The energy balance tells us that the energy of the displaced fluid contributes to the kinetic energy of the ejecta minus potential energies due to gravity  $g$  and surface tension  $\sigma$

$$\rho \left( \frac{\pi}{2} l^2 + 2lh \right) \frac{V_0^2}{2} = \rho \delta H \frac{V_e^2}{2} - \rho \delta \frac{H^2}{2} g - 2\sigma H, \quad (3)$$

where we assumed that the ejecta deflection from the vertical is not substantial, cf. Figure 3, and neglected the energy losses since we are interested in the ejecta formation, which happens over short times and thus dissipation in the low-viscosity fluid (water) used in our experiments is not substantial.

Neglecting the ejecta retraction due to surface tension for a moment, which will be accounted for later, gravity and air entrainment, from Eqs. (1)–(3) we arrive at the following relations for the ejecta velocity, thickness, and height:

$$V_e \sim V_0 \frac{l}{h}, \quad (4a)$$

$$\delta \sim \frac{\sigma}{\rho V_0^2} \frac{h^2}{l^2} = \frac{1}{We} \frac{h^2}{l}, \quad (4b)$$

$$H \sim \frac{\rho V_0^2}{\sigma} \frac{l^3}{h} = We \frac{l^2}{h}, \quad (4c)$$

respectively, where we omitted numerical factors and introduced the Weber number  $We = \rho V_0^2 l / \sigma$ . The deduced relations make qualitative sense: for example, in (4a) the longer the impactor (larger  $l$ ), the larger the pressure gradient between the center  $O$  of the plate and its edge  $S$  and thus the higher the velocity  $V_e$ ; also, the shallower the impact (smaller  $h$ ), the less the amount of mass to be accelerated and thus the higher its velocity, which is consistent with the pressure-impulse theory<sup>2,4</sup> predicting an infinite speed as  $t \rightarrow +0$  (and thus  $h \rightarrow 0$ ). Same conclusions apply to (4b) and (4c), e.g., the shallower the impact the thinner the ejecta, which is observed in experiments indirectly as the rim radius becomes smaller. Similar intuitive arguments can be made about other dependencies on the impact speed  $V_0$ , surface tension  $\sigma$ , density  $\rho$ , and impactor length  $2l$ .

With the determined relations (4a)–(4c) we can now address the question on the conditions under which the pancake forms. First, let us estimate the maximum rim radius  $r$ , which can be done with the help of the Taylor<sup>5</sup>–Culick<sup>6</sup> analysis. Given the Taylor–Culick velocity  $U_{TC} \sim \sqrt{\sigma/(\rho \delta)}$  characteristic of retraction of a liquid sheet of thickness  $\delta$  due to surface tension, the mass balance gives  $U_{TC} \tau_{\text{char}} \delta \sim r^2$ , where the characteristic time over which the rim (and thus the pancake) develops is on the order of the ejecta formation, i.e.,  $\tau_{\text{char}} \sim H/V_e$ ; thus  $r \sim \sqrt{lh}$ , whose dependence on the impactor length  $2l$  and the impact depth  $h$  makes sense as the larger the displaced mass  $\sim lh$ , that is, the deeper the impact and the longer the impactor, the more mass contributes to the rim. No dependence on  $V_0$  is also consistent with the weak variation of  $r$  with  $V_0$  in the experimental observations, cf. Figure 5(b).

Therefore, the transitions from “no pancake to pancake” and from “pancake to corrugations” in Figure 4(a) can be first explained in simple terms (e.g., for fixed plate width  $w$  and impact depth  $h$ ) based on the observation that the characteristic time of the rim formation scales as  $\tau_{\text{char}} \sim V_0$  with the impact velocity  $V_0$ . Thus, the larger  $V_0$ , the more time is given for the pancake formation, which brings us to the (np-p) transition; for even larger  $V_0$  (and thus  $\tau_{\text{char}}$ ), Rayleigh-Plateau instability has

a chance to develop, which is responsible for the (p-c) transition. A more detailed understanding of these transitions is as follows.

First, *the transition* from the pancake to the corrugation (upper transition in Figure 4(a)) occurs when the characteristic time of the pancake formation  $\tau_{\text{char}} \sim H/V_e \sim (\rho V_0/\sigma)l^2$  becomes shorter than that of the Rayleigh-Plateau instability  $\tau_{\text{RP}} \sim \sqrt{\rho r^3/\sigma}$  of the rim,  $\tau_{\text{char}} \lesssim \tau_{\text{RP}}$ , i.e.,

$$\frac{\rho V_0^2}{\sigma} \lesssim \left(\frac{h^3}{l^5}\right)^{1/2} \quad \text{or} \quad We \lesssim \left(\frac{h}{l}\right)^{3/2}, \quad (5)$$

which is also qualitatively consistent with observations. Namely, the higher the impact velocity, the thinner and higher the ejecta and the more well-developed the rim instability, which brings us to the “corrugation” regime, cf. the transition curve (p-c) in Figure 4(a). Also, the more shallow the impact (or the higher the impact speed  $V_0$ ), the thinner the ejecta and thus the rim is thinner as well; and, since the wavelength of the rim instability is related to its diameter – the thinner the rim, the shorter the instability wavelength (of course, this 2D analysis cannot capture the fact that the wider the impactor, the longer the rim and thus more instability wavelengths fit in). Thus, in order to get a pancake instead of a corrugation one needs to increase the impact depth  $h$ , according to (5), or shorten the impactor width  $w$ , cf. Figure 4(a).

As for *the transition* from “no pancake to pancake” (lower transition in Figure 4(a)), it is more difficult to quantify as the pancake is formed much later after the short impact stage and thus the relevant physical variables become complicated functions of the initial conditions and time. However, this transition can be explained based on the observation made earlier that pancake forms if the fluid flux from under the plate along the rim  $V_r r^2$  towards its center (cf. Figure 6) overcomes the mass flux to the rim due to the ejecta retraction  $U_{\text{TC}} \delta l$ . Taking  $V_r = \alpha V_0$  as the velocity at the base of the ejecta gives us

$$\frac{\rho V_0^2}{\sigma} \gtrsim \frac{1}{\alpha l} \quad \text{or} \quad We \gtrsim \frac{1}{\alpha}, \quad (6)$$

that is, enough inertia is needed to get a pancake. While  $\alpha$  is an unknown function of  $h$ ,  $l$ , and time, Figure 4(b) suggests that the deeper  $h$ , the lower  $V_0$  one needs to get a pancake. The latter is easy to understand from the point of view of inertia, namely, the deeper the impact, the lower  $V_0$  is required to provide the same fluid inertia necessary for the pancake formation.

The above minimal 2D model allows one to get an insight into the physics of the pancake formation, in particular the “np-p” and “p-c” transitions in Figure 4, and qualitatively (in the sense of trends) agrees with observations. Should one want to develop a quantitative predictive theory capable of collapsing the data in Figures 4 and 5, one needs to address a number of effects neglected here such as the presence of trapped air and three-dimensionality of the ejecta due to a finite size of the impact plate, all of which have a major influence on the impact phenomena. Whether such an analytical theory can be deduced or not is an open question requiring further exploration.

In conclusion, as follows from the reported experiments and the developed physical intuition, the observed phenomena of singular structures on liquid rims occur when the size and speed of the impacting body are such that the capillary effects become important, e.g., if measured by the Weber number this happens at the lower bound  $We = O(10^2)$  as one can see from Figure 4(a); in the case of water impact,  $We = 10^2$  corresponds to  $l = O(1)$  cm if  $V_0 = 1$  m/s and  $l = O(1)$  m if  $V_0 = 0.1$  m/s. The latter numbers are the realistic practical scales when the effects studied in the present work should be important to keep in mind if, for example, one performs experiments on slamming/planning of ships or landing of airplanes on the water surface scaled down to the extent such that capillarity starts playing a role.

This work was partially supported by the National Science Foundation (NSF) CAREER award under Grant No. 1054267 and American Chemical Society (ACS) Petroleum Research Fund under Grant No. 51307-ND5.

<sup>1</sup> V. I. Arnold, V. V. Goryunov, O. V. Lyashko, and V. A. Vasil'ev, *Singularity Theory I* (Springer-Verlag, New York, 1998).

<sup>2</sup> G. K. Batchelor, *An Introduction to Fluid Dynamics* (Cambridge University Press, Cambridge, 1967).

- <sup>3</sup>Especially taking into account that a pancake forms much later after the impact, when many events have taken place resulting in a complicated flow.
- <sup>4</sup>M. A. Lavrentiev and B. V. Schabat, *Methoden der komplexen Funktionentheorie* (Deutscher Verlag der Wissenschaften, Berlin, 1967).
- <sup>5</sup>G. I. Taylor, "The dynamics of thin sheets of fluid. II. Waves on fluid sheets," *Proc. R. Soc. London, Ser. A* **253**, 296–312 (1959).
- <sup>6</sup>F. E. C. Culick, "Comments on a ruptured soap film," *J. Appl. Phys.* **31**, 1128–1129 (1960).